Update year of Hogg and Hughes reference.

1.9 Friction and Bottom Drag.

Fluid viscosity and frictional drag have been tacitly ignored to this point, an omission that speaks more to the difficulty of including such effects than to their lack of importance. For example, the no-slip condition (v=0) at the bottom of the channel ruins the possibility that the velocity v can be z-independent, or even x-independent if channel sidewalls are considered. The computation of bottom and sidewall viscous boundary layers generally requires numerical methods even when the flow is laminar. Most geophysical and engineering applications involve Reynolds numbers that are much larger than the ($O(10^3)$) threshold required for turbulence. These difficulties have led civil engineers to parameterize the effects of friction through the use of drag laws that date back to the 19th century and were obtained through observations of the Mississippi River and various rivers in Europe (Chow, 1959).

Drag laws introduce a depth-averaged frictional stress into the y-momentum equations. The horizontal velocity v remains z- and x-independent as before. The most common drag law employed in oceanography and meteorology involves a body force in a direction opposite to the fluid motion and proportional to the square of the fluid velocity. The momentum equation (1.3.1) is replaced by

$$\frac{\partial v}{\partial t} + v\frac{\partial v}{\partial y} + g\frac{\partial d}{\partial y} = -g\frac{\partial h}{\partial y} - C_d\frac{v|v|}{d}, \qquad (1.9.1)$$

where C_d is a dimensionless drag coefficient, nominally of order 10^{-3} in sea straits.

If the flow is steady, a solution can be found by integrating (1.9.1) from an upstream point y_o of known velocity and depth to the point y where the solution is desired. The result of this integration can be written

$$\frac{Q^2}{2d(y)^2 w(y)^2} + g[d(y)+h(y)] = \frac{v(y_o)^2}{2} + g[d(y_o)+h(y_o)] - C_d\int_{y_o}^{y}\frac{v(y')|v(y')|}{d(y')}dy' \qquad (1.9.2)$$

The continuity relation $Q = v(y)d(y)w(y) = v(y_o)d(y_o)w(y_o)$ has been used to replace $v(y)$ on the left hand side. The presence of the integral means that the flow state at y depends on the entire history of the flow between y_o and y, and not just the values of the geometric variables h and w at y. The non-local nature of the relationship between the flow and the topography means that (1.9.2) is not of the form sought by Gill (see equation 1.5.1).

In view of the failure of Gill's formalism, we might ask whether any of the concepts we have developed, including subcritical and supercritical flow, hydraulic control and the like, have any meaning or importance when friction is present. Some insight into this question can be gained by writing (1.9.1) and continuity equation (1.3.1) in characteristic form. Following the method established in Section 1.3, the characteristic equations are

$$\frac{d_{\pm}R_{\pm}}{dt} = -g\frac{dh}{dy} - C_d\frac{v^2}{d} \mp \frac{(gd)^{1/2}v}{w}\frac{dw}{dy} \qquad (1.9.3)$$

where

$$\frac{d_{\pm}}{dt} = \frac{\partial}{\partial t} + c_{\pm}\frac{\partial}{\partial y},$$

$R_{\pm} = v \pm 2(gd)^{1/2}$, and $c_{\pm} = v \pm (gd)^{1/2}$ as usual. Solutions to initial value problems can be constructed by integrating (1.9.3) along characteristic curves given by $dy_{\pm}/dt = c_{\pm}$, just as described in Section 3.1. Although the Riemann functions $R_{\pm}$ are not conserved, the characteristic curves still represent paths along which information travels. The characteristic speeds $c_{\pm}$ continue to represent speeds at which information travels and it therefore remains meaningful to classify the flow as being critical, supercritical, and subcritical flow according as $v - (gd)^{1/2} > 0$, $=0$, or <0. This all falls apart, of course, if the frictional term involves derivatives of the flow variables in the y-direction.

A geometrical constraint on the location of a critical section in a steady flow can be found by the steady form of (1.9.3) for R_- by c_-, giving

$$\frac{\partial R_-}{\partial y} = \frac{-g\dfrac{dh}{dy} - C_d\dfrac{v^2}{d} + \dfrac{(gd)^{1/2}v}{w}\dfrac{dw}{dy}}{c_-}$$

The existence of a well behaved solution at a critical section requires that the denominator vanish, and therefore

$$-(dh/dy)_c - C_d + v_c^2(gw_c)^{-1}(dw/dy)_c = 0, \qquad (1.9.4)$$

where the subscript 'c' indicates evaluation at the critical section. If w is constant, (1.9.4) reduces to the simple condition that the critical section must lie where the bottom slope equals the negative of the drag coefficient. Friction therefore tends to shift the control section from the sill to a point downstream, where the bottom slope is negative. If the bottom is horizontal and only the width varies, then critical flow must occur where the channel widens ($dw/dy > 0$).

Some indication of the importance of friction can be gained by comparing the drag and advective terms in (1.9.1). For flow with characteristic depth D passing over an obstacle or through a contraction with y-length L,

$$\frac{C_d \dfrac{v^2}{d}}{v\dfrac{\partial v}{\partial y}} \approx O(C_d L / D) \qquad (1.9.5)$$

and thus friction is significant when $C_d L / D = O(1)$. Friction is typically ignored in simple models of deep ocean overflows and it is an embarrassing fact that estimates of $C_d L / D$ for these flows often exceed unity , even when conservative values of C_d are used. The accompanying table contains some estimates.

Table of values of $C_d L/H$ for 9 oceanographically important straits. L is the strait length, D is the average thickness of the overflowing layer, and C_d is assigned the conservative value 10^{-3}.

Sea Strait	$D(m)$	$L(m)$	$C_d L/H$
Strait of Gibraltar Outflow	2×10^2	2×10^4	0.1
Vema Channel	3×10^2	2×10^5	0.7
Bornholm Strait	30	2.5×10^5	0.8
Bab al Mandab Outflow	10^2	1.5×10^5	4.5
Denmark Strait	5×10^2	5×10^5	1.0
Ecuador Trench	3×10^2	3×10^5	1.0
Faroe Bank Channel	3×10^2	6×10^5	2.0
Bosphorus	20	2×10^4	1.0

Bottom drag can lead to some interesting departures from the steady behavior we have previously discussed. Some of these changes are evident in Figures 1.9.1a,b, which give a comparison between two sets of steady solutions, the first with C_d=0 and the second with C_d >0. Each solution has the same volume flux and the channel width is constant. Solutions are obtained by choosing y_o as the upstream edge of an obstacle, specifying the value B of the Bernoulli function there, and solving (1.9.1) for the fluid depth at successively larger values of y. Each curve is labeled with the nondimensional

value of B. The family of solutions with finite drag has a subcritical-to-supercritical and a supercritical-to-subcritical flow. The flow is critical where the two curves cross each other and, as suggested above, this point lies downstream of the sill. Purely subcritical and supercritical solutions also exist, but these no longer have the upstream/downstream symmetry of their inviscid counterparts. Note that the subcritical solution suffers a reduction in depth as it passes the obstacle, creating the impression of fluid spilling over the sill. The reduction in depth is a consequence of the loss of energy that the fluid experiences as it crosses the topography. Under subcritical conditions the Bernoulli function is dominated by the potential energy $g(d+h)$ and thus a significant depletion of energy must come at the cost of potential energy. The spilling character that a subcritical flow can take on when bottom drag is significant can lead one to mistake the solution for a hydraulically controlled flow.

Some channels contain flow that remains subcritical throughout and evolves mainly due to frictional processes. In fact, a large drag coefficient or sufficiently weak variation in channel geometry may preclude (1.9.4) from ever being satisfied. A simple example would be a constant width channel in which the maximum negative value of the bottom slope is less than C_d. Such cases are sometimes referred to as being *frictionally controlled*, though the term 'control' in this context is ambiguous. Simple models of such flow assume that the channel cross-section and elevation are uniform, in which case analytical solutions may be found. An example is presented in Exercise 1.

It is possible to move beyond the 'slab', in which the bottom drag is distributed equally over the otherwise inviscid water column, to a more realistic model with vertical shear. The assumption of gradual variations in y maintained and thus the pressure remains hydrostatic, but now vertical shear is allowed. The horizontal momentum equation becomes

$$v\frac{\partial v}{\partial y} + w\frac{\partial v}{\partial z} = -g\frac{\partial d}{\partial y} - g\frac{\partial h}{\partial y} + \frac{\partial \tau}{\partial z}. \qquad (1.9.6)$$

where τ is the horizontal shear stress per unit mass. The local condition of incompressibility

$$\frac{\partial v}{\partial y} + \frac{\partial w}{\partial z} = 0$$

implies the existence of a streamfunction ψ such that $\partial\psi / \partial y = -w$ and $\partial\psi / \partial z = v$.

It is possible to express (1.9.6) in the form

$$\frac{\partial B(\psi, y)}{\partial y} = \frac{\partial \tau}{\partial z}, \qquad (1.9.7)$$

as described in Exercise 3. The Bernoulli function $B(\psi, y) = \frac{1}{2}v^2 + gd + gh$ now varies throughout the fluid, though it is conserved along streamlines if the frictional term on the right-hand side is absent. Following Garrett (2004) we may attempt to formulate a Gill type functional for the flow beginning with the trivial relation

$$d = \int_h^{h+d} dz = \int_0^Q \frac{d\psi}{v},$$

where we have assumed the boundary conditions $\psi = (0, Q)$ at $z=(h,d+h)$. Use of the definition of the Bernoulli function to substitute for u allows this relation can be expressed as

$$d - \int_0^Q \frac{d\psi}{2^{1/2}[B(\psi, y) - gd - gh]^{1/2}} = 0. \qquad (1.9.8)$$

If the fluid is inviscid, B is a function of ψ alone and may be considered prescribed by the upstream conditions. Under this condition the only remaining dependent variable in is the depth d and the right hand side is of the desired form. Setting its derivative with respect to d to zero leads to

$$1 = \int_0^Q g \frac{d\psi}{2^{3/2}[B(\psi, y) - gd - gh]^{3/2}} = \int_0^Q g \frac{d\psi}{v^3} = \int_h^{h+d} g \frac{dz}{v^2}$$

and thus the average over the water column of the square of the inverse Froude number must be unity for the flow to be hydraulically critical

$$\frac{1}{d}\int_h^{h+d} \left(\frac{gd}{v^2} \right) dz = 1. \qquad (1.9.9)$$

A remarkable aspect of this condition is that it apparently applies to any stationary wave, including waves that propagate on the vertical vorticity gradients in the flow. However, the coordinate transformation that makes the derivation possible assumes a one-to-one relationship between ψ and z, and this hold only when v does not change sign. It is possible that critical conditions with respect to certain wave modes are more general than (1.9.9).

The addition of frictional dissipation to our sheared flow means that B varies along streamlines and can no longer be prescribed by conditions far upstream. Because of the unknown y-dependence in $B(\psi,y)$, the left side of (1.9.8) no longer fits Gill's definition of a hydraulic function. However we may still use this relation to formulate a critical condition, provided that the dissipation takes a particular form. Consider a hypothetical flow over varying topography that becomes critical at a particular section $y=y_c$. Criticality specifically means that the flow at $y=y_c$ can support a stationary,

infinitesimal disturbance and that this disturbance can exist only at $y=y_c$. This definition is consistent with the inviscid examples considered elsewhere in this chapter, but it has yet to be shown that the postulated state is dynamically consistent in the presence of dissipation. In order for it to be so, the disturbance at $y=y_c$ must clearly be isolated and cannot contaminate the flow upstream. This assumption can be supported if the dissipation depends on the local properties of the flow at y_c and not, say, on the derivatives of the flow fields with respect to y. Thus if $\partial\tau / \partial z$ in (1.9.6) takes the form $\nu\partial^2 v / \partial z^2$, where ν is a molecular viscosity, the assumption is justified. In this case the disturbed flow at $y=y_c$ has the same $B(\psi,y_c)$ as the undisturbed flow, the latter being set by conditions occurring in $y<y_c$ where the disturbance is not present. The stationary wave at y_c then involves a perturbation in d that satisfies (1.9.6) for a fixed $B(\psi,y_c)$. The critical condition in this case is therefore identical to the inviscid condition (1.9.9). On the other hand, a dissipation form that contains derivatives in y or otherwise gives rise to non-local information may invalidate the assumptions. Let us assume that this is not the case and proceed forward.

If the (1.9.6) is differentiated with respect to y and the critical condition applied the result may be written as

$$\int_h^{h+d} \frac{\partial \tau}{\partial z} u^{-2} dz - \frac{dh}{dy} = 0 .$$

Integrating the first term by parts leads after rearrangement to

$$\frac{dh}{dy} = \left[\frac{\tau}{v^2} \right]_{z=h+d} - \left[\frac{\tau}{v^2} \right]_{z=h} + 2\int_h^{h+d} \frac{\tau}{v^3} \frac{\partial v}{\partial z} dz .$$

The previous two expressions are evaluated at $y=y_c$. If the stress at the free surface is zero, the first term vanishes. The bottom stress term is just what is parameterized by the drag coefficient C_d in slab models. Finally the expression $\tau\partial v / \partial z$ may be regarded as the internal rate of energy dissipation and is often denoted by ε. With these substitutions, the last expression may be written as

$$\frac{dh}{dy} = -C_d + 2\int_h^{h+d} \frac{\varepsilon}{v^3} dz . \qquad (1.9.10)$$

It follows that the action of bottom drag alone causes the control section to lie where the bottom slope is the negative of the drag coefficient, as found by Pratt (1987) in connection with the slab model. Surprisingly, internal dissipation gives rise to the opposite tendency.

Hogg and Hughes (2006) have calculated numerical solutions for free surface flows with constant molecular viscosity and an example is shown in Figure 1.9.2 (Hogg's Fig. 1). The usual no-slip boundary condition at the bottom is replaced by specification of the bottom stress in the form

$$\tau_{z=h} = C_d v_{z=h}^2 . \qquad (1.9.11)$$

The fluid is therefore free to slip over the bottom with horizontal velocity $v_{z=h}$ and the drag coefficient and molecular viscosity are specified independently. This artificial setting is concession to more realistic applications in which the viscosity is a parameterization of turbulence and where the exact form of the bottom boundary condition is unknown. The numerical solution shown has uniform velocity upstream of the obstacle and has the appearance of an inviscid, hydraulically controlled flow (panel *a* of Figure 1.9.2). The flow passes through a critical section at a point slightly downstream of the sill where left-hand side of (1.9.9), which can be interpreted as a generalized Froude number, passes though unity (solid curve in *b*). The velocity field and the velocity profile at the control section (*c*) shows the development of vertical shear as the fluid spills over the sill. The development of shear leads to higher rates of depth averaged internal dissipation (dashed line in *b*).

An illuminating exercise in assessing the validity of slab models is to fix the drag coefficient, vary the viscosity, and note the behavior of the resulting velocity profiles. If the upstream conditions are fixed as in the previous experiment, C_d is held fixed at value 10^{-2}, and ν is varied over 6 orders of magnitude, a set of differing critical-section velocity profiles is obtained (Figure 1.9.3, Hogg's Figure 3). For small viscosity, the shear is concentrated in a thin bottom boundary layer (*a*). As ν is increased the boundary layer grows (*b*) and the shear becomes distributed over the whole depth (*c* and *d*). Even larger values of ν smooth the velocity over the whole water column leading to a depth-independent profile (*e*). The flow is therefore slab like in the limit of low and high viscosity. Hogg and Hughes also find that the position of the control is generally dominated by the bottom drag term in (1.9.10).

Exercises

1) For flow in a channel with constant h and w, show that bottom friction causes the flow to evolve in the downstream direction towards criticality.

2) Consider a strait with constant w and h connecting two infinitely wide reservoirs. The flow in the strait is subcritical and subject to quadratic bottom drag but no entrainment.

(a) Assuming that the strait extends from y=0 to y=L, find a general algebraic expression relating the depth d to the position y. Calculate the drop in the level of the surface (or interface) between the ends of the strait as a function of d(0) and the transport Q.

(b) Show that the only possible location for critical flow must be at the ends of the strait, where w changes from a finite value to infinity.

(c) Find the solution that is critical at y=0 and show that the surface (or interface) slope is infinite there.

(Further discussion and an application of this procedure to two-layer flow can found in Assaf and Hecht, 1974.)

3) For the vertically sheared flow described by equation (1.9.6) suppose that the variables u and w are expressed in terms of the coordinates ψ and y (rather than z and y)**.** By transforming the right hand side to the new variables, show that (1.9.7) holds.

Figure Captions

1.9.1 Steady solutions for flow over an obstacle with height h_m* with constant volume flux ($Q/gh_m^{3/2}w$*=1) and various values of the Bernoulli function B*$/gh_m$. The solutions in (a) have no bottom drag whereas those in (b) have a drag equivalent to C_dL/h_m=0.5.

1.9.2 Numerical solution for a viscous free surface flow over an isolated obstacle with ν=$10^{-2}m^2/s$, C_d=10^{-2} and uniform upstream velocity. Streamlines are shown in (a) while the Froude number (right-hand term in 1.9.9, solid line) and depth average internal dissipation ε are shown in (b). The inset shows the Froude number in the vicinity of the critical section. Panel (c) shows the velocity v and, in the inset, the velocity profile at the critical section. (Hogg and Hughes, 200? Fig. 1)

1.9.3 A sequence of velocity profiles, measured at the critical section and obtained from numerical experiments of the type shown in Figure 1.9.2. The upstream conditions and the constant drag coefficient C_d=10^{-2} are fixed. The viscosity is varied as indicated in each frame. (Hogg and Hughes, 200? Fig. 3.)

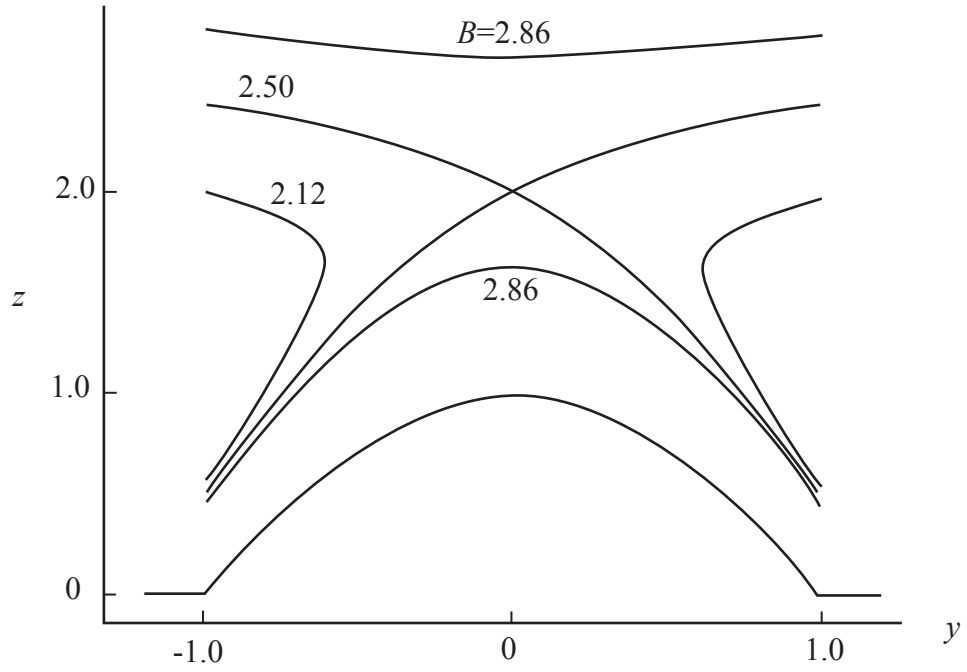

(a)

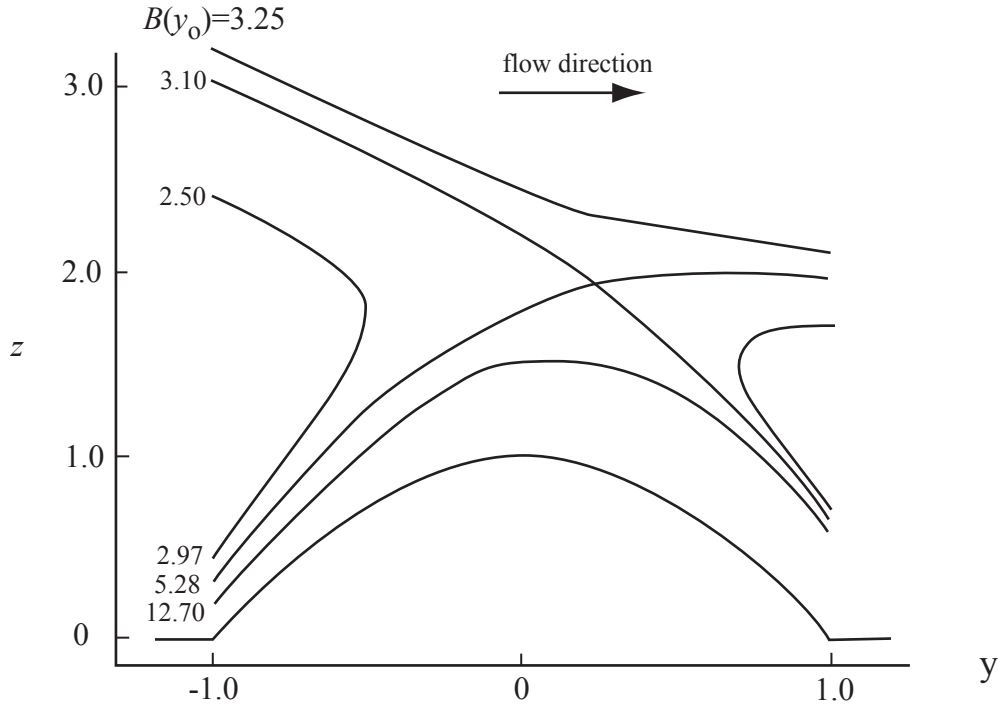

(b)

Figure 1.9.1

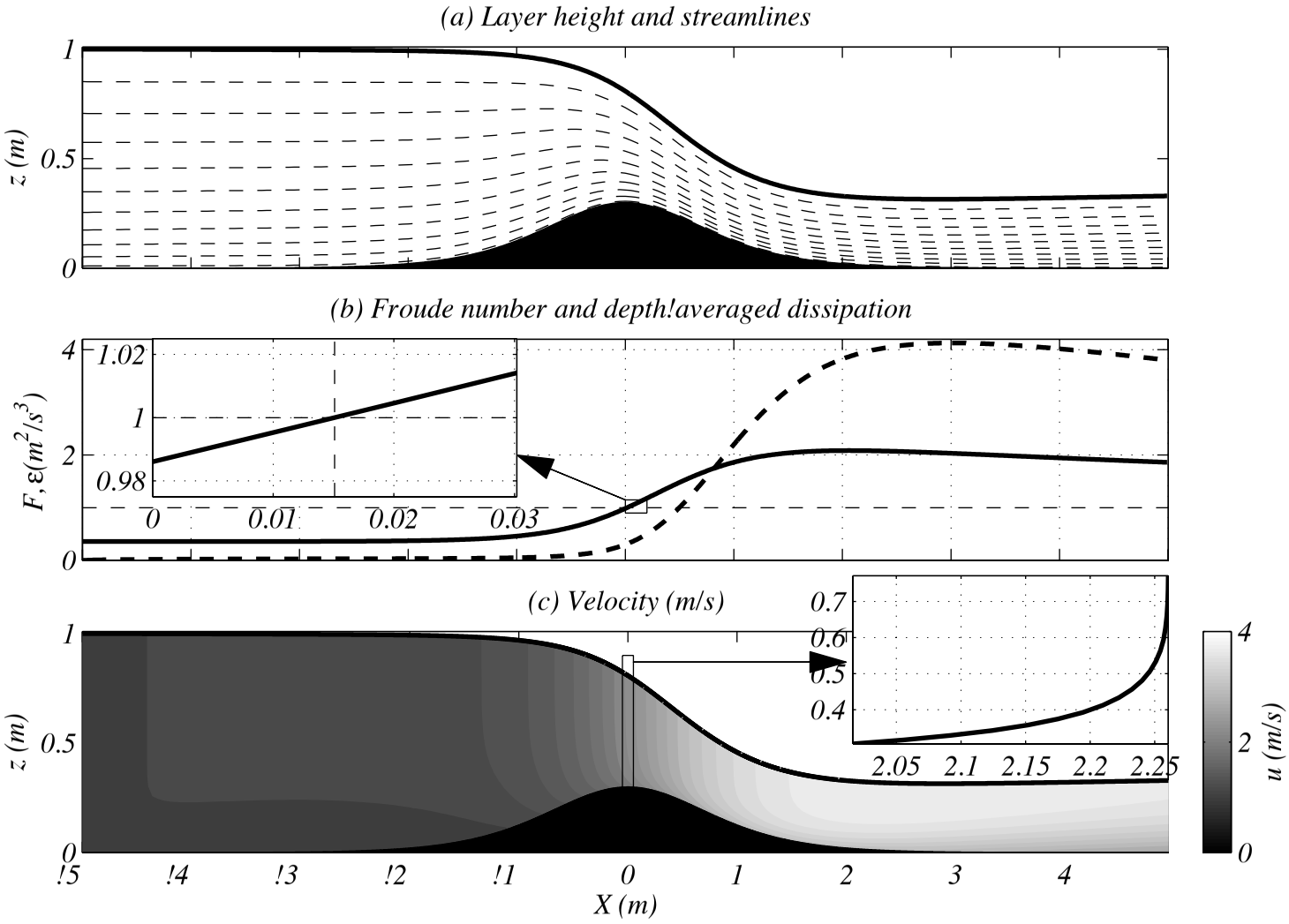
(a) Layer height and streamlines
z (m)
1
0.5
0
(b) Froude number and depth!averaged dissipation
F, ε(m²/s³)
4
2
0
1.02
1
0.98
0
0.01
0.02
0.03
(c) Velocity (m/s)
z (m)
1
0.5
0
0.7
0.6
0.5
0.4
2.05
2.1
2.15
2.2
2.25
4
2
0
u (m/s)
!5
!4
!3
!2
!1
0
1
2
3
4
X (m)

Figure 1.9.2

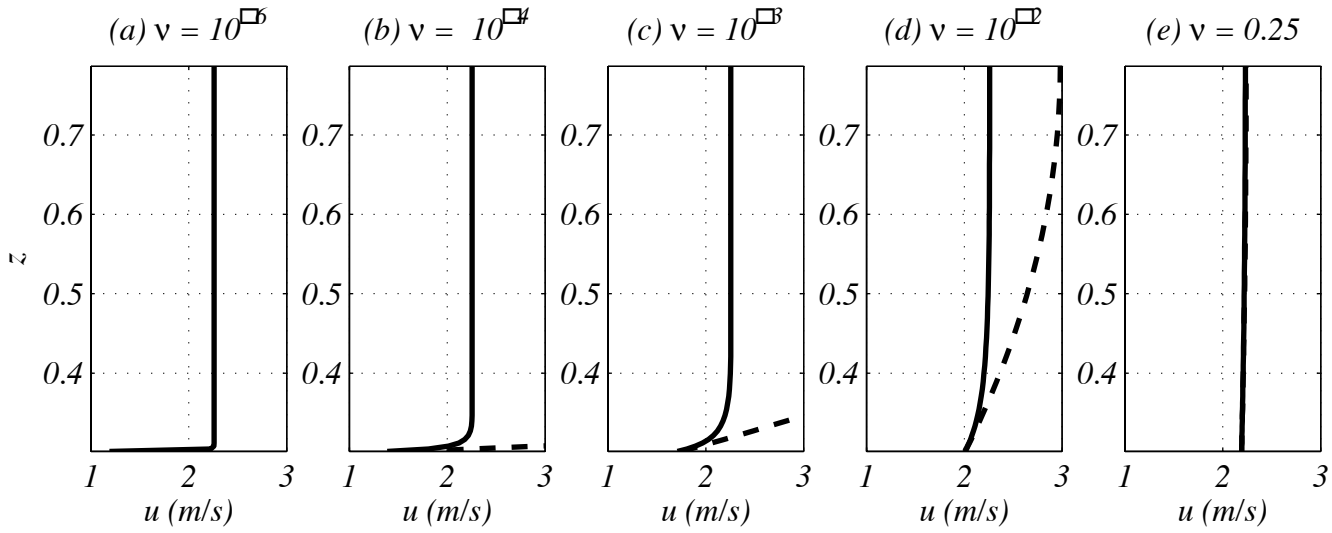

Figure 1.9.3